Enhancement of valley-selective excitation by a linearly polarized two-color laser pulse

Arqum Hashmi,[1] Shunsuke Yamada,[1] Kazuhiro Yabana,[1,2] and Tomohito Otobe[1,*]
[1]*Kansai Photon Science Institute, National Institutes for Quantum Science and Technology (QST), Kyoto 619-0215, Japan*
[2]*Center for Computational Sciences, University of Tsukuba, Tsukuba 305-8577, Japan*

(Received 27 March 2023; revised 23 May 2023; accepted 24 May 2023; published 6 June 2023)

Here, we propose valley-selective excitations via a two-color ($\omega + 2\omega$) laser field, made by superimposing two linearly polarized pulses at frequencies ω and 2ω. We have studied the intensity ratio between a few-cycle pulse of an ω and 2ω laser, and its enhancement factor by employing time-dependent first-principles calculations. The valley polarization depends on the carrier-envelope phases (CEPs) of the pulses and the intensity ratio $I_\omega/I_{2\omega}$. We found that a two-color field enhances valley polarization by as much as 1.2 times larger than a single-color pulse. Maximum valley asymmetry is achieved for an intensity ratio $I_\omega/I_{2\omega}$ of 36 with a relative CEP of π. In our previous work, we found that the asymmetric vector potential induces valley polarization [A. Hashmi *et al.*, Phys. Rev. B **105**, 115403 (2022)]. In this paper, we find that the asymmetry of the electric field modulates the valley polarization. Our two-color scheme offers another path toward the optical control of valley pseudospins.

DOI: 10.1103/PhysRevB.107.235403

I. INTRODUCTION

Electrons in two-dimensional (2D) hexagonal lattices have an extra degree of freedom in addition to a charge and spin named the valley pseudospin [1,2]. Valleys are local minima in the band structure corresponding to different crystal momenta that are located at the K/K' points of the Brillouin zone (BZ) [3,4]. In the field of valleytronics, extensive research efforts are being applied to 2D layer materials such as graphene [5,6] and transition metal dichalcogenides (TMDs) [7–9]. Graphene presents a remarkable feature of Dirac fermions [10,11]. However, a honeycomb structure with equivalent A and B sublattices enforces zero Berry curvature which makes it not an ideal candidate for valley contrasting properties [12]. As opposed to graphene, TMD monolayers are of particular interest for practical valleytronics applications because of their broken inversion symmetry and strong spin-orbit coupling (SOC).

Lifting valley degeneracy to create valley polarization has become a central theme in valleytronics [13–15]. Several methods have been proposed to achieve transient valley polarization such as applying a magnetic field [16], optical Stark effect [17], by doping [18,19], and proximity effects generated by magnetic substrates [20]. Due to several practical limitations of the magnetic field, optical excitations remain a popular way where the selective excitation at K or K' can be achieved using a weak circularly polarized field resonant with the band gap of the material [8,21,22]. Depending on its helicity, the field couples to either K/K' valleys.

The valley-dependent optical selection rules suggest that linearly polarized light couples equally to both valleys. It is widely accepted that valley polarization with linearly polarized fields is impossible [4,23]. In contrast, it is expected that a few-cycle (one to three cycles) single-color pulse with the controlled carrier-envelope phase (CEP) can break this situation [24,25]. Moreover, ultrashort laser pulses offer ultrafast control of electron dynamics [26,27]. The possibility of generating valley polarization with linearly polarized pulses offers an alternative route to valleytronics in graphene and TMD materials [24,28]. The advantage of linearly polarized pulses is to avoid reliance on resonant pump-probe spectroscopy that is used in TMD monolayers to break the symmetry between the K and K' valleys.

Electron dynamics under a strong laser field can be described by solving the time-dependent Kohn-Sham (TDKS) equation in real time, referred to as time-dependent density functional theory (TDDFT) [29,30]. TDDFT has not only been used to describe the linear response in the frequency domain [31,32] but also has been very successful to describe the nonlinear and nonperturbative dynamics of electrons by intense ultrashort laser pulses [33–35]. The most powerful aspect of TDDFT is its capability to describe electron dynamics under intense laser fields without any empirical parameters. In condensed matter, it is well known that SOC modifies the band structure of solids. Strong SOC not only modifies the band curvature but also changes the band gap of the material by lifting the spin degeneracy, which ultimately can affect the excitation of carriers. Hence the inclusion of SOC in TDDFT is essential not only to describe the excitation dynamic under a strong laser field but also important to accurately describe phenomena such as spintronics [36] or valleytronics [14].

In our previous study, we found that an asymmetric laser field with a monocycle laser pulse enables valley polarization by the real-time TDDFT approach with SOC [25]. A two-color laser can also control the asymmetric excitation [37–40]. In this paper, we study the enhancement of valley polarization in a WSe_2 monolayer via a two-color field. It is possible to create an asymmetric laser field by mixing a fundamental laser pulse with frequency ω and its second harmonic 2ω. The two-pulse intensity ratio and the relative CEP control the valley polarization. We also compare the valley polarization

*otobe.tomohito@qst.go.jp

results of the $\omega + 2\omega$ scheme with a single-color (ω) pulse. We found that the valley polarization via two-color control exceeds the single-color scheme by 1.2 times as the $\omega + 2\omega$ field exhibits more asymmetry in its temporal shape.

II. THEORETICAL FORMALISM

Using the velocity gauge [41], we describe the time evolution of electron orbitals in a WSe_2 monolayer under a pulsed electric field by solving the TDKS equation for Bloch orbitals $u_{b,\mathbf{k}}(\mathbf{r},t)$ (which is a two-component spinor; b is the band index and $\mathbf{k}$ is the 2D crystal momentum of the thin layer) as

$$i\hbar\frac{\partial}{\partial t}u_{b,\mathbf{k}}(\mathbf{r},t) = \left[\frac{1}{2m}\left(-i\hbar\nabla + \hbar\mathbf{k} + \frac{e}{c}\mathbf{A}^{(t)}(t)\right)^2 - e\varphi(\mathbf{r},t) + \hat{v}_{\mathrm{NL}}^{\mathbf{k}+\frac{e}{\hbar c}\mathbf{A}^{(t)}(t)} + v_{\mathrm{xc}}(\mathbf{r},t)\right]u_{b,\mathbf{k}}(\mathbf{r},t), \tag{1}$$

where the scalar potential $\varphi(\mathbf{r},t)$ includes the Hartree potential from the electrons plus the local part of the ionic pseudopotentials and we have defined $\hat{v}_{\mathrm{NL}}^{\mathbf{k}} \equiv e^{-i\mathbf{k}\cdot\mathbf{r}}\hat{v}_{\mathrm{NL}}e^{i\mathbf{k}\cdot\mathbf{r}}$. Here, $\hat{v}_{\mathrm{NL}}$ and $v_{\mathrm{xc}}(\mathbf{r},t)$ are the nonlocal part of the ionic pseudopotentials and exchange-correlation potential, respectively.

A TDKS equation combined with Maxwell equations can describe the light propagation in thin layers as well. For this purpose, we assume a spatially uniform macroscopic electric field inside the layer (in our case the monolayer is in the xy plane and the light pulse propagates along the z axis) [42,43]. By using Maxwell equations, the propagation of macroscopic electromagnetic fields in the form of the vector potential $\mathbf{A}(z,t)$ is described as

$$\left(\frac{1}{c^2}\frac{\partial^2}{\partial t^2} - \frac{\partial^2}{\partial z^2}\right)\mathbf{A}(z,t) = \frac{4\pi}{c}\mathbf{J}(z,t), \tag{2}$$

where $\mathbf{J}(z,t)$ is the macroscopic current density of the thin layer.

Under the assumption of zero thickness and a spatially uniform electric field inside the monolayer, we can approximate the macroscopic electric current density in Eq. (2) as

$$\mathbf{J}(z,t) \approx \delta(z)\mathbf{J}_{2\mathrm{D}}(t), \tag{3}$$

where $\mathbf{J}_{2\mathrm{D}}(t)$ is the 2D current density (current per unit area of the thin layer). In Eq. (3), $\delta(z)$ is the Dirac delta function. It is treated as the boundary value problem in solving Eq. (2) providing connection conditions among incident, reflected, and transmitted fields at $z = 0$. The explicit form of $\mathbf{J}_{2\mathrm{D}}(t)$ is given as follows,

$$\mathbf{J}_{2\mathrm{D}}(t) = -\frac{e}{m}\int dz\int_{\Omega}\frac{dxdy}{\Omega}\sum_{b,\mathbf{k}}^{\mathrm{occ}} u_{b,\mathbf{k}}^{\dagger}(\mathbf{r},t) \times\left[-i\hbar\nabla + \hbar\mathbf{k} + \frac{e}{c}\mathbf{A}^{(t)}(t) + \frac{m}{i\hbar}\left[\mathbf{r}, \hat{v}_{\mathrm{NL}}^{\mathbf{k}+\frac{e}{\hbar c}\mathbf{A}^{(t)}(t)}\right]\right] \times u_{b,\mathbf{k}}(\mathbf{r},t), \tag{4}$$

where Ω is the area of the 2D unit cell and the sum is taken over the occupied orbitals in the ground state. Details of our formalism are explained in Refs. [25,42].

The method explained above is implemented in the TDDFT package called scalable *ab initio* light-matter simulator for optics and nanoscience (SALMON). Full details of the SALMON code and its implementation are described elsewhere [44,45].

The lattice parameter of the WSe_2 monolayer is chosen to be 3.32 Å. A vacuum distance of 20 Å was employed in the direction normal to the interface. The exchange-correlation potential utilizes the adiabatic local-density approximation with the Perdew-Zunger functional [46]. We use a spin noncollinear treatment for the exchange-correlation potential [47,48]. The dynamics of the 12 valence electrons for one W atom, and 12 valence electrons for two Se atoms are treated explicitly while the effects of the core electrons are considered through norm-conserving pseudopotentials [49]. The total energy convergence criterion was set to 10^{-8} eV. For such calculations, the spatial grid sizes and k points are optimized. The converged results were obtained with a fine r grid and k grid of 0.21 Å and $15 \times 15 \times 1$ k mesh, respectively. We use the vector potential for the fundamental laser pulse and its second harmonic pulses with the following waveform,

$$A(t) = -\frac{c}{\omega}f(t)\left[E_\omega\cos\left\{\omega\left(t - \frac{T_P}{2}\right) + \varphi_\omega\right\} + \frac{1}{2}E_{2\omega}\cos\left\{2\omega\left(t - \frac{T_P}{2}\right) + \varphi_{2\omega}\right\}\right], \tag{5}$$

where E_ω and $E_{2\omega}$ are the peak electric field amplitudes while φ_ω and $\varphi_{2\omega}$ are CEPs of the fundamental pulse and its second harmonic, respectively. ω is the carrier frequency and T_P is the total pulse duration. The pulse envelope function is of $\cos^4$ shape for the vector potential given as

$$f(t) = \begin{cases}\cos^4\left(\pi\frac{t-T_P/2}{T_P}\right), & 0 \leqslant t \leqslant T_P,\\ 0, & \text{otherwise.}\end{cases} \tag{6}$$

We use linearly polarized pulses with 0.4 eV frequency for the fundamental pulse and its second harmonic (0.8 eV). Both pulse lengths are set to $T_P = 10$ fs and a small time step size of 5×10^{-4} fs is used for stable calculations.

III. RESULTS AND DISCUSSION

For the molecules, asymmetric behavior with an intensity ratio $I_\omega/I_{2\omega}$ around four has been used with a photon energy far below the ionization potential [37,38]. Here, I_ω and $I_{2\omega}$ are the intensities of the ω and 2ω pulses, respectively. Since we assume frequencies comparable to the band gap of WSe_2, the electronic response is significantly different for ω and 2ω. Therefore, we have to clarify the electron dynamics under each color field before proceeding with the two-color field.

Figure 1(a) shows the vector potential of both pulses. A field intensity of $I = 10^{10}$ W/cm^2 is used for ω and 2ω pulses, and the laser intensity is chosen to induce the nonlinear dynamics but be below the damage threshold for monolayer TMDs [50,51]. In our previous study, we have shown that the polarization parallel to Γ-K experiences a different band curvature and hence induces a high degree of valley polarization that can be controlled by CEP [25]. Thus the direction of the polarization of the incident light is considered along Γ-K. Figure 1(b) displays the excitation dynamics regarding

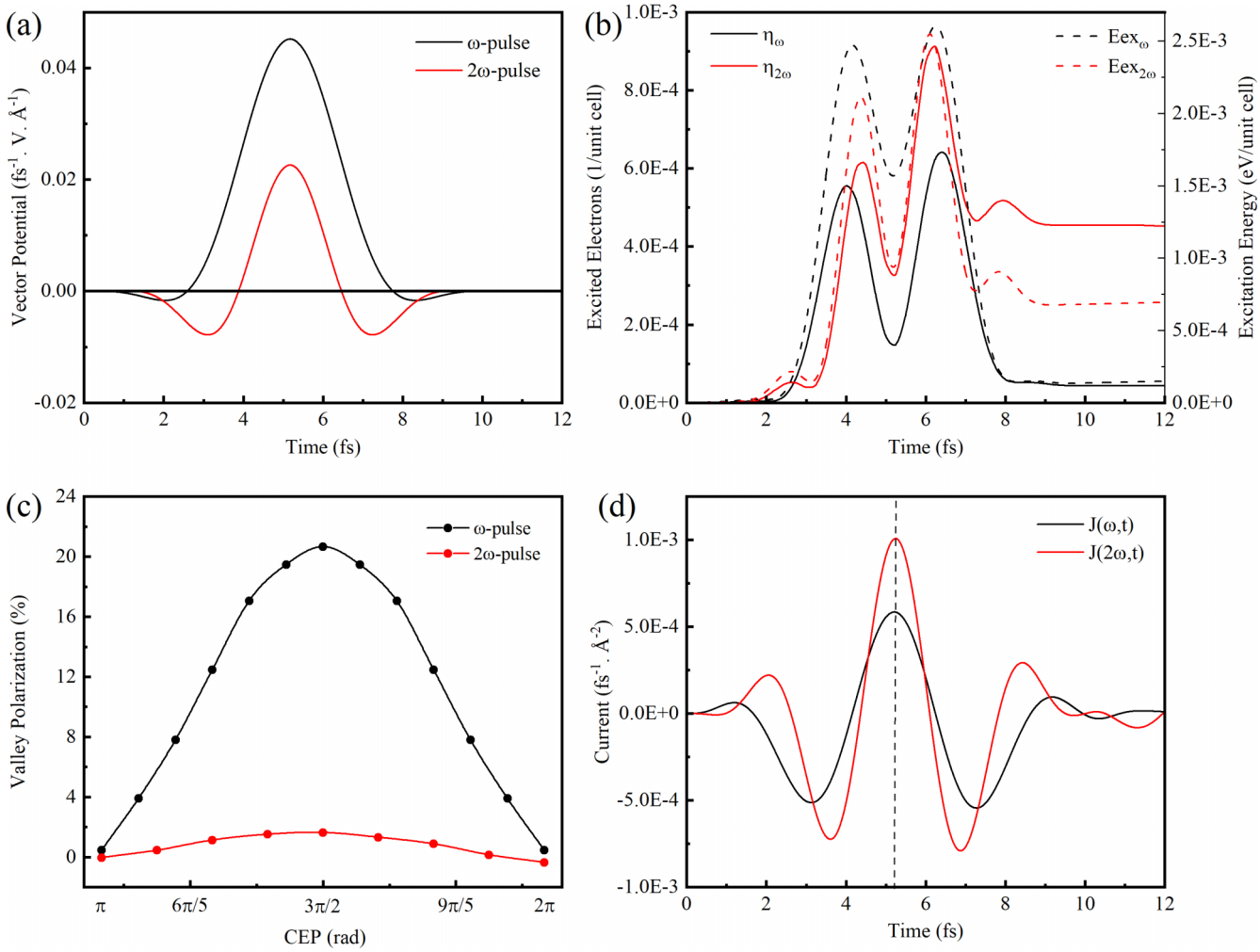

FIG. 1. Comparison of two single-color laser fields with frequencies of ω and 2ω. Both pulses have an intensity of 10^{10} W/cm^2. (a) The vector potential. (b) The temporal development of excitation energies (Eex) and excited electrons (η). (c) Valley polarization as a function of CEP and (d) the temporal evolution of photocurrents. The CEP in (a), (b), and (d) is $3\pi/2$.

excitation energy and excited electrons. In the case of an ω field, the excitation energy and the excited electrons are noticeable during the pulse irradiation, and the electronic state returns to its ground state when the pulse ends. The energy per electron is about 8 photons (3.16 eV/electron), which is higher than the expected lowest excitation path (4 photons). On the other hand, in the case of a 2ω field, more electrons are excited as compared to ω and the excited electrons remain finite after the pulse ends. The absorbed energy per electron is about 1.52 eV/electron, which indicates the lowest order of the photoabsorption, the two-photon absorption, is dominant. The Keldysh parameter is around 2 for the ω field and 4 for the 2ω field. These results suggest that the excitation process under the ω field is highly nonlinear than 2ω, and is in the intermediate stage between multiphoton and tunneling processes.

Figure 1(c) shows a comparison of the valley polarization by the ω and 2ω fields. The valley polarization is defined as

$$\text{Polarization} = \frac{\rho_{K'} - \rho_K}{\frac{1}{2}(\rho_{K'} + \rho_K)}, \tag{7}$$

where ρ_K ($\rho_{K'}$) are electron densities, obtained by integrating the conduction band electron population around the K (K') point. Strong valley polarization is observed by the ω pulse while the 2ω field does not show any significant valley polarization. The photocurrent indicates the sensitivity of the system for each frequency, shown in Fig. 1(d). The current ratio for 2ω is roughly twice that of the ω pulse. The large difference in the photocurrent between the 2ω and ω pulses indicates that we have to find a good ratio $I_\omega/I_{2\omega}$ to enhance the asymmetric valley polarization.

According to our previous work [25], the valley polarization with a monocycle pulse shows a peak with a phase of $\varphi = \pi/2$ and $3\pi/2$. Regarding the relative phase (φ_{rel}), an intense asymmetric response of molecules has been reported with 0 and π [52]. Figure 2(a) shows the valley polarization by changing the E_ω field while $E_{2\omega}$ is fixed at 10^{10} W/cm^2, that is, an intense 2ω pulse case. The CEPs are set as $\varphi_\omega = \pi/2$ and $\varphi_{2\omega} = 3\pi/2$ to induce the best valley polarization. Intense 2ω results in two-photon absorption, which leads to the K and K' valleys being equally excited. Hence no valley asymmetry is present in this case.

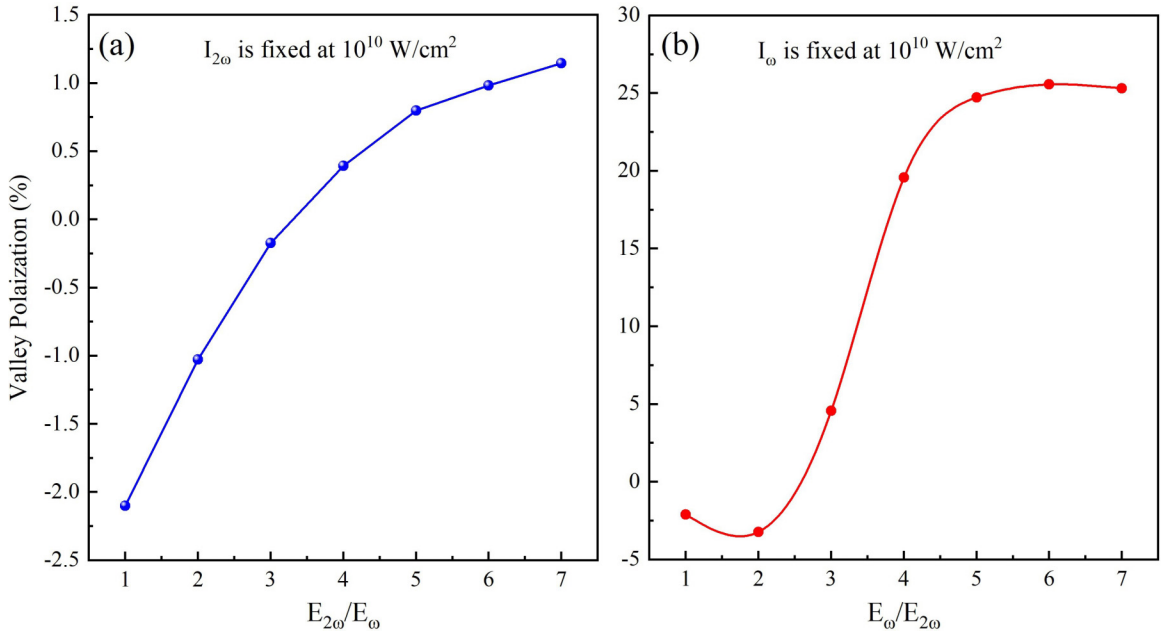

FIG. 2. Valley polarization of the two-color field ($\omega + 2\omega$) field as the function of the ratio between the electric field strengths. (a) The field strength of ω is varied while 2ω is fixed. The CEP is fixed at $\varphi_\omega = \pi/2$ and $\varphi_{2\omega} = 3\pi/2$. (b) The field strength of 2ω is varied while ω is fixed. The CEP is fixed at $\varphi_\omega = 3\pi/2$ and $\varphi_{2\omega} = \pi/2$. The CEPs are chosen to have a positive peak of valley polarization.

Figure 2(b) shows the valley polarization by changing $E_{2\omega}$ with intense E_ω. The valley polarization increases as $E_{2\omega}$ decreases, which distinctly indicates the change in the excitation process from the two-photon absorption to tunneling. Figure 2 confirms that a maximum valley polarization is observed for an $E_\omega/E_{2\omega}$ ratio of 6. A ratio of field $E_\omega/E_{2\omega} = 6$ corresponds to an intensity ratio of $I_\omega/I_{2\omega} = 36$. It should be noted that the ratio $I_\omega/I_{2\omega} = 4$, which is the ratio used in the molecule case, does not work [Fig. 2(b)]. For further calculations, we have fixed the laser intensity of the fundamental pulse to $I_\omega = 1 \times 10^{10}$ W/cm^2 while the superimposed $\omega + 2\omega$ optimized ratio $I_\omega/I_{2\omega}$ is fixed to 36.

Before going into details of the valley polarization by $\omega + 2\omega$, we present a schematic diagram of the valley-selective excitation mechanism by linearly polarized two-color laser pulses in Fig. 3. The valley polarization in the case of $\omega + 2\omega$ depends on the dynamics of the excited carriers. Linearly polarized pulses can excite electrons either by multiphotonic absorption or via the tunneling process. According to Figs. 1(c) and 2(a), an intense 2ω field induces two-photon absorption and small valley polarization. In the case of the ratio $I_\omega/I_{2\omega} = 1$ [Fig. 3(a)], multiphoton absorption at the K and K' valleys occurs equally because the 2ω field is relatively intense. As we have reported, the tunneling effect is the key process in valley polarization with a linear polarized laser. As the ratio $I_\omega/I_{2\omega}$ increases, the character of a longer wavelength field, ω field, should appear. Figures 3(b) and 3(c) show the schematic explanation for why the tunneling process under an asymmetric field induces valley polarization. The asymmetric vector potential exploits the asymmetric band curvature of the WSe_2 monolayer with respect to the K/K' point. The vector potential of the laser field corresponds to the intraband motion and the intraband trajectories of electrons at the K/K' valleys are different as shown in Figs. 3(b) and 3(c). The transition dipole moment can be approximated as a function of inverse reduced mass [53,54]. The asymmetric intraband dynamics in asymmetric band curvature (i.e., effective mass) results in valley polarization. It should be noted that the interference of the wave packet with an extremely intense field also affects valley polarization [25].

Next, we investigate the distribution of excited-state electrons in reciprocal space. The excited electron population is defined as

$$\rho_{\mathbf{k}}(t) = \sum_{c,v} \left| \int_\Omega d^3r\, u^*_{v,\mathbf{k}}(\mathbf{r},t) u^{\mathrm{GS}}_{c,\mathbf{k}+\frac{e}{\hbar c}\mathbf{A}^{(t)}(t)}(\mathbf{r}) \right|^2, \tag{8}$$

where v and c are the indices for the valence and conduction bands, respectively, and $u^{\mathrm{GS}}_{b,\mathbf{k}}(\mathbf{r}) = u_{b,\mathbf{k}}(\mathbf{r}, t = 0)$ is the Bloch orbital in the ground state.

Figure 4(b) shows the maximum population asymmetry at the K and K' valley corresponds to the vector potential shown in Fig. 4(a). One can see that a positive vector potential favors the K' valley. As the φ_ω changes from $3\pi/2$ to $\pi/2$ the waveform of the vector potential changes from positive to negative as shown in Fig. 4(c). Reversing the φ of the ω pulse [$-\pi/2$ ($3\pi/2$) â' $\pi/2$] and switching the valley asymmetry from the K' to K valley as shown in Fig. 4(d) suggests a robust mechanism for valley selection.

Figure 5(a) shows the valley polarization as a function of the $\varphi_{2\omega}$ at numerous CEPs of φ_ω. As described above, no asymmetry is observed at $\varphi_\omega = 0$. Consequently, the valley polarization is zero regardless of $\varphi_{2\omega}$. The valley polarization increases as we change φ_ω. The valley polarization has an order of $\varphi_\omega = 3\pi/2 > \varphi_\omega = 1.625\pi > \varphi_\omega = 7\pi/4$ and the maximum value is as high as 26%. Valley polariza-

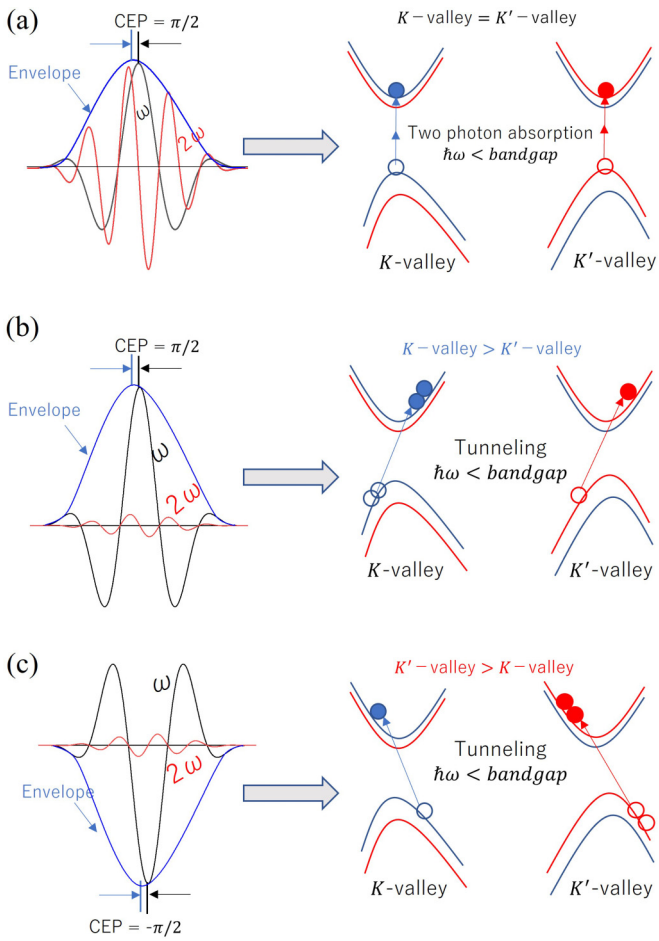

FIG. 3. Schematic diagram of valley-selective excitation mechanism by linearly polarized two-color laser pulses. The population asymmetry at the K and K' valleys is sensitive to the field strength between the ω and 2ω fields and is further enhanced by optimizing the CEP. Here, three different cases are shown: (a) The excitation process with a ratio of $I_\omega/I_{2\omega} = 1$. (b) The ω and 2ω field with an optimized ratio ($I_\omega/I_{2\omega} = 36$). (c) This case is the same as (b) but the CEP of $\omega + 2\omega$ is the opposite. The left panels indicate the vector potentials and the right panels indicate the band structure and excitation processes.

tion via two-color control exceeds the single-color scheme by 1.2 times as the $\omega + 2\omega$ field exhibits more asymmetry in its temporal shape. An increase in the valley polarization as compared to the single-color value indicates that the addition of the 2ω field significantly affects the valley polarization. The phase dependence of the valley polarization shows that $\varphi_{\rm rel}$ between ω and 2ω is crucial to tune the valley polarization. It is also worth mentioning that the $\varphi_{\rm rel}$ dependence changes according to the phase of the fundamental pulse. The valley polarization dependence on $\varphi_{\rm rel}$ can be explained by the asymmetry of the vector potential and electric field as shown in Figs. 5(b) and 5(c). Here, the asymmetry of the vector potential and the electric field is defined as

$$\mathrm{Asym}_{A(E)} = \left|\frac{A_+(E_+)(t)}{A_-(E_-)(t)}\right|, \tag{9}$$

where $A_\pm(t)$ and $E_\pm(t)$ are the positive (+) and negative (−) peaks of the vector potential and electric field, respectively.

Valley polarization and $\mathrm{Asym}_{A(t)}$ have strong relevance, i.e., a smaller vector potential value produces weaker valley polarization while a higher value of $\mathrm{Asym}_{A(t)}$ results in a stronger valley polarization. In our calculation, the $\mathrm{Asym}_{A(t)}$ (asymmetry of excitation area) dictates the main peak position of valley polarization. However, the peak of the valley polarization may not directly correspond to the maxima of the vector potential. As one can see. the valley polarization peak for $\varphi_\omega = 1.625\pi$ is at 0.625π while the $\mathrm{Asym}_{A(t)}$ peak is at 0.375π of $\varphi_{2\omega}$ in Fig. 5. Similarly for $\varphi_\omega = 7\pi/4$ the valley peak is at $3\pi/4$ while the $\mathrm{Asym}_{A(t)}$ peak is at $\pi/2$ of $\varphi_{2\omega}$. In principle, the peak of valley polarization should follow $\mathrm{Asym}_{A(t)}$ if the tunneling of the electrons is solely responsible for the valley polarization. Even though it is a minor effect, the asymmetric excitation rate due to $E(t)$ influences valley polarization. Since $\mathrm{Asym}_{E(t)}$ is shifted by CEP, the asymmetry of valley polarization shifts slightly by changing CEP.

The peak value of valley polarization in Fig. 5(a) is observed at $\varphi_{2\omega} = \pi/2$, 0.625π, and $3\pi/4$. Thus, we have explored the valley polarization at peaks of $\varphi_{2\omega}$ as a function of φ_ω. Figure 6(a) shows the valley polarization as a function of φ_ω at peaks of $\varphi_{2\omega}$. The valley polarization curve at various $\varphi_{2\omega}$ nearly overlaps. The φ_ω dependence of valley polarization shows the same behavior as in the case of a single-color linearly polarized pulse [24,25], except for an increase in the valley polarization value in the second positive half of the sinelike curve. Thus, this valley polarization increase is due to the 2ω field. The $\mathrm{Asym}_{A(t)}$ in Fig. 6(b) and the $\mathrm{Asym}_{E(t)}$ in Fig. 6(c) show very distinctive curves. Due to the predominant tunneling nature of the ω field, the valley polarization nearly follows the $\mathrm{Asym}_{A(t)}$ curve as shown in Fig. 6(b). The change in the shoulder structure of $\mathrm{Asym}_{E(t)}$ in Fig. 6(c) changes the peak position of valley asymmetry to $\varphi_\omega = 1.625\pi$ for $\varphi_{2\omega} = 0.625\pi$ and $3\pi/4$ which marks the importance of $\mathrm{Asym}_{E(t)}$ by the $\omega + 2\omega$ field. Thus the competition between the asymmetry of the excitation rate and excitation area by the addition of a 2ω field determines the peak of valley polarization.

Detectability is a crucial aspect of this study and two methods for experimentally detecting valley polarization have been reported: luminescence and the valley Hall effect [4]. According to previous optical spectroscopy and time-resolved photoluminescence experiments [55,56], the valley lifetime is in the order of picoseconds (several picoseconds). Here, ultrashort femtosecond laser pulses have been used to create valley polarization on a femtosecond timescale much shorter than the carrier lifetime. The ability to control the valley dynamics on a suboptical cycle opens the possibility to control the ultrafast electron dynamics in TMDs. In the case of the valley Hall effect, the laser spot size should be comparable to the target to avoid intervalley scattering [57]. Lastly, note that the polarization and phase-controlled bichromatic pulses have been successively used to control the angular emission distribution in molecules [58,59] and the photocurrent in 2D materials [39,60]. These works suggest that our proposed idea of valley-selective excitation by a two-color laser is certainly achievable experimentally.

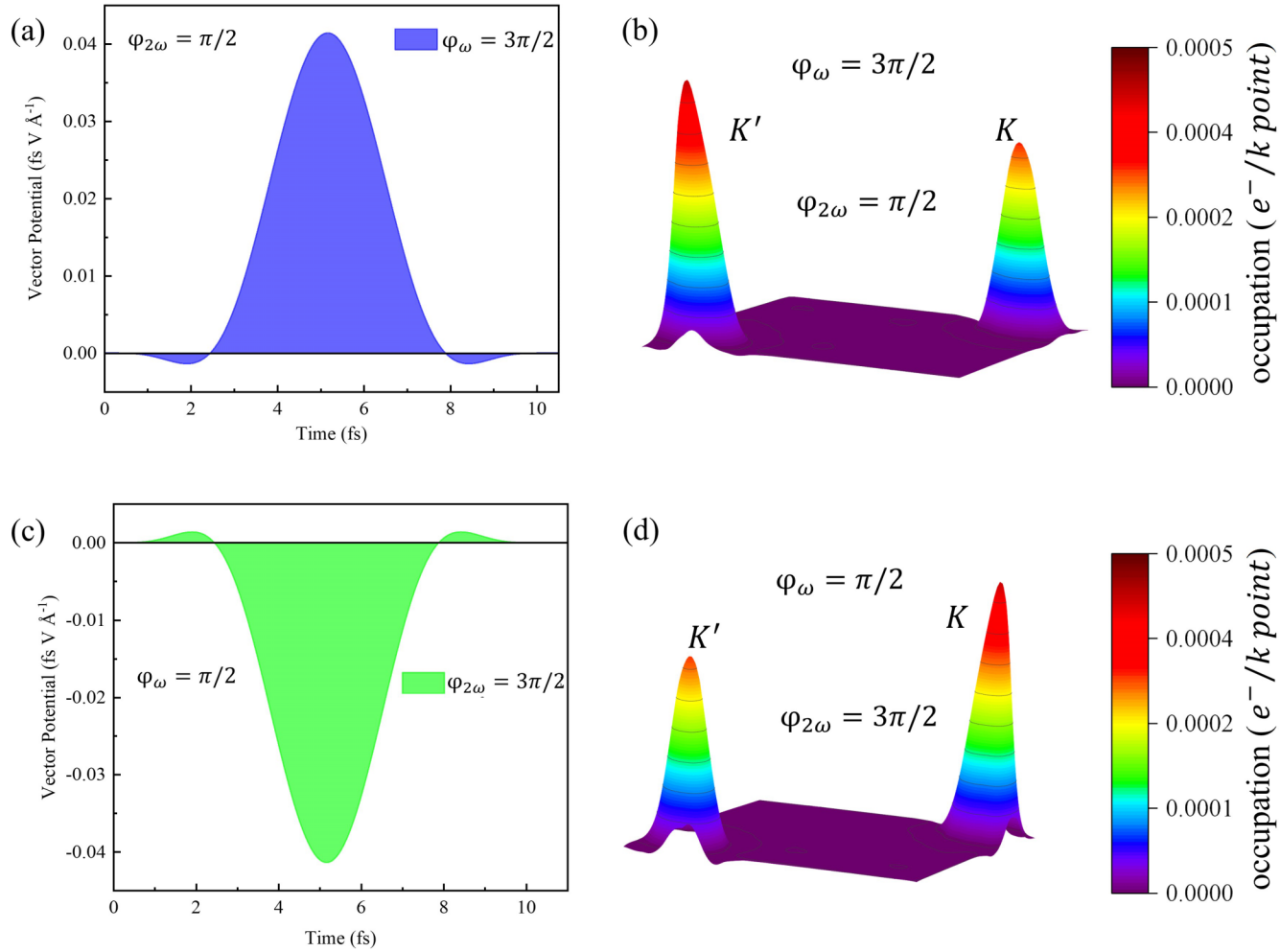

FIG. 4. (a) Vector potential of the $\omega + 2\omega$ field for φ_ω $3\pi/2$ and $\varphi_{2\omega}$ $\pi/2$. (b) Conduction band electron populations for the vector potential in (a). (c) and (d) are the same as (a) and (b) but for $\varphi_\omega = \pi/2$, $\varphi_{2\omega} = 3\pi/2$. The electron population is summed over the entire conduction band at the end of the pulse. Two waveforms and their corresponding k-resolved populations are chosen because of their maximum asymmetry and the switching of the valley from K' to K.

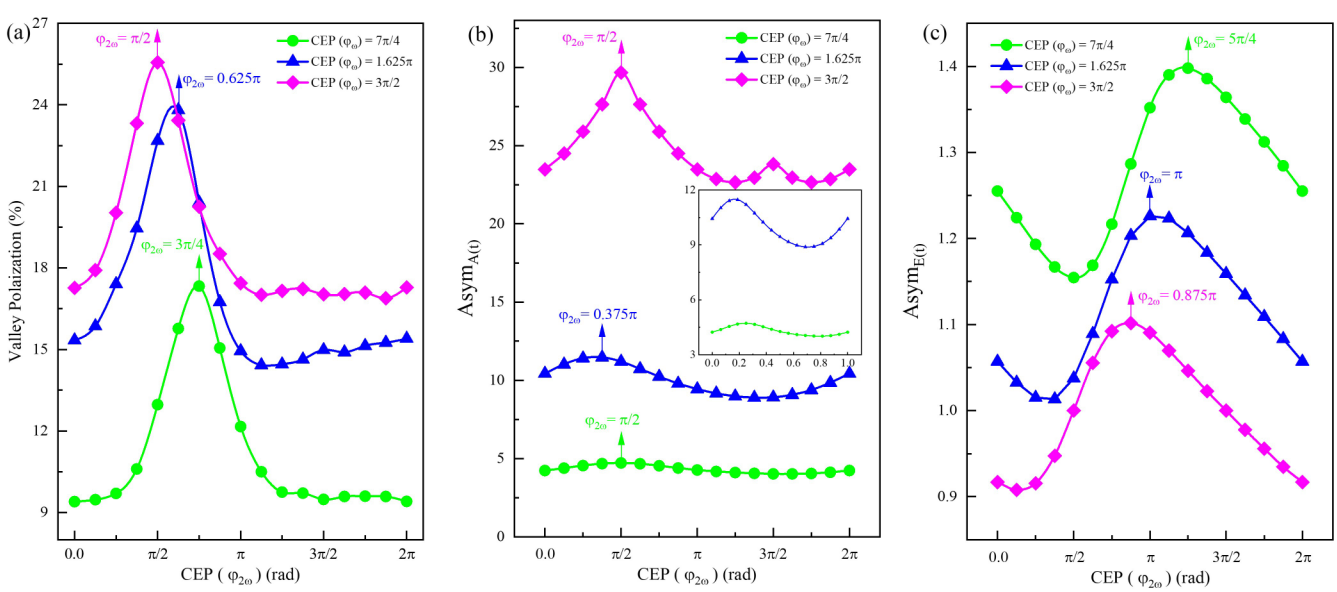

FIG. 5. (a) Valley polarization. (b) Asym$_{A(t)}$ and (c) Asym$_{E(t)}$ as a function of $\varphi_{2\omega}$ at a specific CEP of ω. The intensity of $I_{\omega+2\omega} = 0.01$ TW cm^{-2} while $I_\omega/I_{2\omega} = 36$.

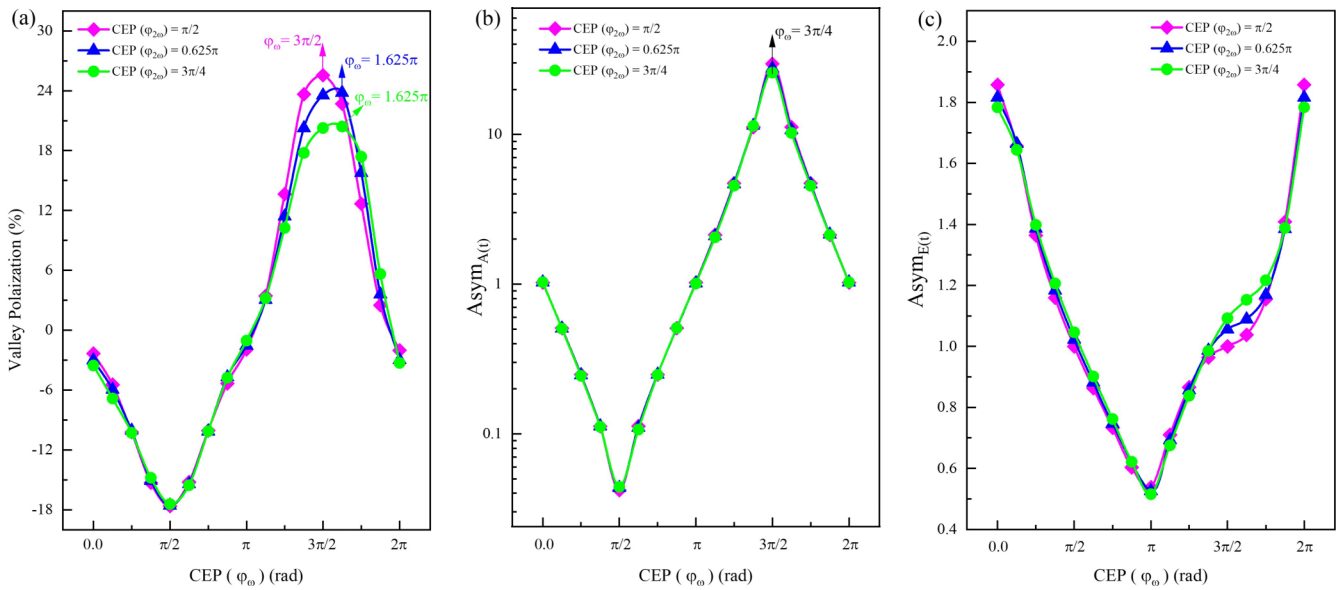

FIG. 6. (a) Valley polarization. (b) Asym$_{A(t)}$ and (c) Asym$_{E(t)}$ as a function of φ_ω at a maximum valley polarization of $\varphi_{2\omega}$ in Fig. 5(a).

IV. CONCLUSION

We have demonstrated the generation of valley polarization in a WSe_2 monolayer via $\omega + 2\omega$ superimposed collinear laser pulses. The valley polarization induced by $\omega + 2\omega$ pulses is superior to a single-color pulse by as much as 1.2 times. The intensity ratio and the relative phase between the fundamental pulse and its second harmonic are the most crucial factors in determining valley polarization. Our results indicate that a strong ω mixed with a weaker 2ω enhances the valley polarization. We found that the ratio of $I_\omega/I_{2\omega} = 36$ shows higher valley polarization than the ratio used in molecule cases. The valley polarization is mainly dependent on the CEP of the fundamental pulse. The competition between the asymmetry of the vector potential and electric field mainly determined the maximum valley polarization. Two-color fields provide additional degrees of freedom, such as admixture, polarization, and the relative phase between two pulses. The present scheme helps to understand the ultrafast valley phenomena in 2D layers from a fundamental perspective.

ACKNOWLEDGMENTS

This research is supported by JST-CREST under Grant No. JP-MJCR16N5. This research is also partially supported by JSPS KAKENHI Grants No. 20H02649 and No. 22K13991, and MEXT Quantum Leap Flagship Program (MEXT Q-LEAP) under Grants No. JPMXS0118068681 and JPMXS0118067246. The numerical calculations were carried out using the computer facilities of the Fugaku through the HPCI System Research Project (Project ID hp220120), SGI8600 at Japan Atomic Energy Agency (JAEA), and Multidisciplinary Cooperative Research Program in CCS, University of Tsukuba.

The authors declare no competing financial interest.

[1] D. Xiao, G.-B. Liu, W. Feng, X. Xu, and W. Yao, Coupled Spin and Valley Physics in Monolayers of MoS_2 and Other Group-VI Dichalcogenides, Phys. Rev. Lett. **108**, 196802 (2012).

[2] X. Xu, W. Yao, D. Xiao, and T. F. Heinz, Spin and pseudospins in layered transition metal dichalcogenides, Nat. Phys. **10**, 343 (2014).

[3] Q. H. Wang, K. Kalantar-Zadeh, A. Kis, J. N. Coleman, and M. S. Strano, Electronics and optoelectronics of two-dimensional transition metal dichalcogenides, Nat. Nanotechnol. **7**, 699 (2012).

[4] J. R. Schaibley, H. Yu, G. Clark, P. Rivera, J. S. Ross, K. L. Seyler, W. Yao, and X. Xu, Valleytronics in 2D materials, Nat. Rev. Mater. **1**, 16055 (2016).

[5] D. Xiao, W. Yao, and Q. Niu, Valley-Contrasting Physics in Graphene: Magnetic Moment and Topological Transport, Phys. Rev. Lett. **99**, 236809 (2007).

[6] Y. Shimazaki, M. Yamamoto, I. V. Borzenets, K. Watanabe, T. Taniguchi, and S. Tarucha, Generation and detection of pure valley current by electrically induced Berry curvature in bilayer graphene, Nat. Phys. **11**, 1032 (2015).

[7] E. J. Sie, Valley-selective optical stark effect in monolayer WS_2, in *Coherent Light-Matter Interactions in Monolayer Transition-Metal Dichalcogenides* (Springer, Berlin, 2018), pp. 37–57.

[8] T. Cao, G. Wang, W. Han, H. Ye, C. Zhu, J. Shi, Q. Niu, P. Tan, E. Wang, B. Liu *et al.*, Valley-selective circular dichroism of monolayer molybdenum disulphide, Nat. Commun. **3**, 887 (2012).

[9] A. M. Jones, H. Yu, N. J. Ghimire, S. Wu, G. Aivazian, J. S. Ross, B. Zhao, J. Yan, D. G. Mandrus, D. Xiao *et al.*, Optical generation of excitonic valley coherence in monolayer WSe_2, Nat. Nanotechnol. **8**, 634 (2013).

[10] A. K. Geim, Graphene: status and prospects, Science **324**, 1530 (2009).

[11] A. H. Castro Neto, F. Guinea, N. M. R. Peres, K. S. Novoselov, and A. K. Geim, The electronic properties of graphene, Rev. Mod. Phys. **81**, 109 (2009).

[12] Y. Zhang, Y.-W. Tan, H. L. Stormer, and P. Kim, Experimental observation of the quantum Hall effect and Berry's phase in graphene, Nature (London) **438**, 201 (2005).

[13] H. Yuan, X. Wang, B. Lian, H. Zhang, X. Fang, B. Shen, G. Xu, Y. Xu, S.-C. Zhang, H. Y. Hwang *et al.*, Generation and electric control of spin–valley-coupled circular photogalvanic current in WSe_2, Nat. Nanotechnol. **9**, 851 (2014).

[14] S. A. Vitale, D. Nezich, J. O. Varghese, P. Kim, N. Gedik, P. Jarillo-Herrero, D. Xiao, and M. Rothschild, Valleytronics: opportunities, challenges, and paths forward, Small **14**, 1801483 (2018).

[15] T. Zhang, Y. Ma, X. Xu, C. Lei, B. Huang, and Y. Dai, Two-dimensional valleytronics in single-layer t-ZrNY (Y= Cl, Br) predicted from first principles, J. Phys. Chem. C **124**, 20598 (2020).

[16] D. MacNeill, C. Heikes, K. F. Mak, Z. Anderson, A. Kormányos, V. Zólyomi, J. Park, and D. C. Ralph, Breaking of Valley Degeneracy by Magnetic Field in Monolayer $MoSe_2$, Phys. Rev. Lett. **114**, 037401 (2015).

[17] J. Kim, X. Hong, C. Jin, S.-F. Shi, C.-Y. S. Chang, M.-H. Chiu, L.-J. Li, and F. Wang, Ultrafast generation of pseudo-magnetic field for valley excitons in WSe_2 monolayers, Science **346**, 1205 (2014).

[18] R. Peng, Y. Ma, S. Zhang, B. Huang, and Y. Dai, Valley polarization in Janus single-layer MoSSe via magnetic doping, J. Phys. Chem. Lett. **9**, 3612 (2018).

[19] X. Xu, Y. Ma, T. Zhang, C. Lei, B. Huang, and Y. Dai, Nonmetal-atom-doping-induced valley polarization in single-layer Tl_2O, J. Phys. Chem. Lett. **10**, 4535 (2019).

[20] D. Zhong, K. L. Seyler, X. Linpeng, R. Cheng, N. Sivadas, B. Huang, E. Schmidgall, T. Taniguchi, K. Watanabe, M. A. McGuire *et al.*, Van der Waals engineering of ferromagnetic semiconductor heterostructures for spin and valleytronics, Sci. Adv. **3**, e1603113 (2017).

[21] H. Zeng, J. Dai, W. Yao, D. Xiao, and X. Cui, Valley polarization in MoS_2 monolayers by optical pumping, Nat. Nanotechnol. **7**, 490 (2012).

[22] K. F. Mak, K. He, J. Shan, and T. F. Heinz, Control of valley polarization in monolayer MoS_2 by optical helicity, Nat. Nanotechnol. **7**, 494 (2012).

[23] W. Yao, D. Xiao, and Q. Niu, Valley-dependent optoelectronics from inversion symmetry breaking, Phys. Rev. B **77**, 235406 (2008).

[24] Á. Jiménez-Galán, R. E. Silva, O. Smirnova, and M. Ivanov, Sub-cycle valleytronics: control of valley polarization using few-cycle linearly polarized pulses, Optica **8**, 277 (2021).

[25] A. Hashmi, S. Yamada, A. Yamada, K. Yabana, and T. Otobe, Valley polarization control in WSe_2 monolayer by a single-cycle laser pulse, Phys. Rev. B **105**, 115403 (2022).

[26] F. Langer, C. P. Schmid, S. Schlauderer, M. Gmitra, J. Fabian, P. Nagler, C. Schüller, T. Korn, P. Hawkins, J. Steiner *et al.*, Lightwave valleytronics in a monolayer of tungsten diselenide, Nature (London) **557**, 76 (2018).

[27] P. Kumar, T. M. Herath, and V. Apalkov, Ultrafast valley polarization in bilayer graphene, J. Appl. Phys. **130**, 164301 (2021).

[28] H. K. Kelardeh, U. Saalmann, and J. M. Rost, Ultrashort laser-driven dynamics of massless dirac electrons generating valley polarization in graphene, Phys. Rev. Res. **4**, L022014 (2022).

[29] J. Theilhaber, *Ab initio* simulations of sodium using time-dependent density-functional theory, Phys. Rev. B **46**, 12990 (1992).

[30] K. Yabana and G. F. Bertsch, Time-dependent local-density approximation in real time, Phys. Rev. B **54**, 4484 (1996).

[31] K. Yabana, T. Nakatsukasa, J.-I. Iwata, and G. Bertsch, Real-time, real-space implementation of the linear response time-dependent density-functional theory, Phys. Status Solidi B **243**, 1121 (2006).

[32] A. D. Laurent and D. Jacquemin, TD-DFT benchmarks: A review, Int. J. Quantum Chem. **113**, 2019 (2013).

[33] A. Castro, M. A. L. Marques, J. A. Alonso, G. F. Bertsch, and A. Rubio, Excited states dynamics in time-dependent density functional theory, Eur. Phys. J. D **28**, 211 (2004).

[34] K. Nobusada and K. Yabana, High-order harmonic generation from silver clusters: Laser-frequency dependence and the screening effect of *d* electrons, Phys. Rev. A **70**, 043411 (2004).

[35] T. Otobe, M. Yamagiwa, J.-I. Iwata, K. Yabana, T. Nakatsukasa, and G. F. Bertsch, First-principles electron dynamics simulation for optical breakdown of dielectrics under an intense laser field, Phys. Rev. B **77**, 165104 (2008).

[36] I. Žutić, J. Fabian, and S. D. Sarma, Spintronics: Fundamentals and applications, Rev. Mod. Phys. **76**, 323 (2004).

[37] H. Ohmura, N. Saito, and T. Morishita, Molecular tunneling ionization of the carbonyl sulfide molecule by double-frequency phase-controlled laser fields, Phys. Rev. A **89**, 013405 (2014).

[38] S. Kaziannis, N. Kotsina, and C. Kosmidis, Interaction of toluene with two-color asymmetric laser fields: Controlling the directional emission of molecular hydrogen fragments, J. Chem. Phys. **141**, 104319 (2014).

[39] T. Higuchi, C. Heide, K. Ullmann, H. B. Weber, and P. Hommelhoff, Light-field-driven currents in graphene, Nature (London) **550**, 224 (2017).

[40] Á. Jiménez-Galán, R. Silva, O. Smirnova, and M. Ivanov, Lightwave control of topological properties in 2D materials for sub-cycle and non-resonant valley manipulation, Nat. Photonics **14**, 728 (2020).

[41] G. F. Bertsch, J.-I. Iwata, A. Rubio, and K. Yabana, Real-space, real-time method for the dielectric function, Phys. Rev. B **62**, 7998 (2000).

[42] S. Yamada, M. Noda, K. Nobusada, and K. Yabana, Time-dependent density functional theory for interaction of ultrashort light pulse with thin materials, Phys. Rev. B **98**, 245147 (2018).

[43] S. Yamada and K. Yabana, Determining the optimum thickness for high harmonic generation from nanoscale thin films: An *ab initio* computational study, Phys. Rev. B **103**, 155426 (2021).

[44] M. Noda, S. A. Sato, Y. Hirokawa, M. Uemoto, T. Takeuchi, S. Yamada, A. Yamada, Y. Shinohara, M. Yamaguchi, K. Iida *et al.*, Salmon: Scalable *ab-initio* light–matter simulator for optics and nanoscience, Comput. Phys. Commun. **235**, 356 (2019).

[45] Salmon official, http://salmon-tddft.jp.

[46] J. P. Perdew and Y. Wang, Accurate and simple analytic representation of the electron-gas correlation energy, Phys. Rev. B **45**, 13244 (1992).

[47] U. Von Barth and L. Hedin, A local exchange-correlation potential for the spin polarized case. I, J. Phys. C **5**, 1629 (1972).

[48] T. Oda, A. Pasquarello, and R. Car, Fully Unconstrained Approach to Noncollinear Magnetism: Application to Small Fe Clusters, Phys. Rev. Lett. **80**, 3622 (1998).

[49] I. Morrison, D. M. Bylander, and L. Kleinman, Nonlocal Hermitian norm-conserving Vanderbilt pseudopotential, Phys. Rev. B **47**, 6728 (1993).

[50] H. Liu, Y. Li, Y. S. You, S. Ghimire, T. F. Heinz, and D. A. Reis, High-harmonic generation from an atomically thin semiconductor, Nat. Phys. **13**, 262 (2017).

[51] N. Yoshikawa, K. Nagai, K. Uchida, Y. Takaguchi, S. Sasaki, Y. Miyata, and K. Tanaka, Interband resonant high-harmonic generation by valley polarized electron–hole pairs, Nat. Commun. **10**, 3709 (2019).

[52] H. Ohmura, T. Nakanaga, and M. Tachiya, Coherent Control of Photofragment Separation in the Dissociative Ionization of IBr, Phys. Rev. Lett. **92**, 113002 (2004).

[53] E. Kane, Zener tunneling in semiconductors, J. Phys. Chem. Solids **12**, 181 (1960).

[54] T. Otobe, Y. Shinohara, S. A. Sato, and K. Yabana, Theory for electron excitation in dielectrics under an intense linear and circularly polarized laser fields, J. Phys. Soc. Jpn. **88**, 024706 (2019).

[55] G. Wang, L. Bouet, D. Lagarde, M. Vidal, A. Balocchi, T. Amand, X. Marie, and B. Urbaszek, Valley dynamics probed through charged and neutral exciton emission in monolayer WSe_2, Phys. Rev. B **90**, 075413 (2014).

[56] C. R. Zhu, K. Zhang, M. Glazov, B. Urbaszek, T. Amand, Z. W. Ji, B. L. Liu, and X. Marie, Exciton valley dynamics probed by Kerr rotation in WSe_2 monolayers, Phys. Rev. B **90**, 161302(R) (2014).

[57] K. F. Mak, K. L. McGill, J. Park, and P. L. McEuen, The valley Hall effect in MoS_2 transistors, Science **344**, 1489 (2014).

[58] H. Ohmura, N. Saito, and M. Tachiya, Selective Ionization of Oriented Nonpolar Molecules with Asymmetric Structure by Phase-Controlled Two-Color Laser Fields, Phys. Rev. Lett. **96**, 173001 (2006).

[59] P. V. Demekhin, A. N. Artemyev, A. Kastner, and T. Baumert, Photoelectron Circular Dichroism with Two Overlapping Laser Pulses of Carrier Frequencies ω and 2ω Linearly Polarized in Two Mutually Orthogonal Directions, Phys. Rev. Lett. **121**, 253201 (2018).

[60] C. Heide, T. Boolakee, T. Eckstein, and P. Hommelhoff, Optical current generation in graphene: CEP control vs. $\omega + 2\omega$ control, Nanophotonics **10**, 3701 (2021).